

---

# Human Dosimetry and Biodistribution of Iodine-123-Iododexetimide: A SPECT Imaging Agent for Cholinergic Muscarinic Neuroreceptors

Karyn L. Boundy, Leighton R. Barnden, Christopher C. Rowe, Mark Reid, Michael Kassiou, Andrew G. Katsifis and Richard M. Lambrecht

*Departments of Nuclear Medicine and Neurology, The Queen Elizabeth Hospital, Woodville; and Biomedicine and Health Program, Australian Nuclear Science and Technology Organisation, Menai, Australia*

---

Iodine-123-iododexetimide (IDEX) has recently been used for SPECT imaging of muscarinic cholinergic neuroreceptors (mAChR) in humans. We report the human radiation dosimetry, whole-body and normal cerebral distribution of IDEX. **Methods:** Serial whole-body planar and brain SPECT scans were performed over 24 hr in four normal subjects. Organ activity was calculated from attenuation-corrected geometric mean counts from ROIs drawn over visible organs. Thigh activity was used for background subtraction. Organ absorbed doses and effective dose were calculated using the MIRL schema. Brain SPECT was performed 6 hr postinjection in ten normal subjects. ROIs placed over cortical and subcortical structures were used to determine brain distribution. **Results:** The effective dose was 24.7  $\mu\text{Sv}/\text{MBq}$ . An average of 54% of IDEX remained in the body background. Decay-corrected brain uptake was 6.9% of injected dose at 1 hr, 8.6% at 6 hr and 8.1% at 24 hr. Regional brain distribution showed high uptake in striatum and cortex with low activity in thalamus and cerebellum. At 6 hr, activity relative to striatum was 70% for frontal and parietal cortex, 102% for occipital cortex, 54% for thalamus and 11% for cerebellum. **Conclusion:** Iodine-123-IDEX produced high quality SPECT images with activity at 6 hr reflecting the known distribution of mAChR receptors. The favorable dosimetry of IDEX and high synthetic yield (50%–70%) suggest it to be a suitable agent for clinical studies.

**Key Words:** iodine-123-iododexetimide; radiation dosimetry; muscarinic cholinergic neuroreceptors; single-photon emission computed tomography

**J Nucl Med 1995; 36:1332–1338**

---

**T**he cholinergic neurotransmitter system plays an important role in memory and other cognitive functions (1) and is

involved in a number of neuro-degenerative diseases, including Alzheimer's disease, Parkinson's disease and Huntington's chorea (2). Disease-related neuroreceptor changes have been determined in postmortem brain tissue, usually at end-stage disease. There is sparse information on in vivo receptor status in the earlier stages of neurodegenerative disease.

Several PET ligands have been assessed for human in vivo study of muscarinic cholinergic receptors (mAChR), including  $^{11}\text{C}$ -quinuclidinyl benzilate (QNB) (3),  $^{11}\text{C}$ -cogentin (4),  $^{11}\text{C}$ -scopolamine (5),  $^{18}\text{F}$ -2-fluorodexetimide and  $^{18}\text{F}$ -4-fluorodexetimide (6). Because PET scanning has limited availability, an  $^{123}\text{I}$ -labeled mAChR neuroreceptor ligand for SPECT would be useful.

SPECT mAChR imaging was first performed in humans in 1985 with  $^{123}\text{I}$ -QNB by Holman (7) and a number of studies have been performed with this agent (8). Radiosynthesis of  $^{123}\text{I}$ -QNB with high specific activity is difficult and the synthetic yield is less than 20% (9).

An alternate SPECT radioligand for mAChR is  $^{123}\text{I}$ -iododexetimide (IDEX) synthesized at Johns Hopkins University in 1989 (10). It is derived from dexetimide, a long-acting anticholinergic drug previously used in the treatment of Parkinson's disease and tardive dyskinesia.

Dexetimide, the D-isomer, has stereospecific high affinity for the mAChR (11) and can be displaced by centrally acting anticholinergic medications (12). On the other hand, levetimide, the L-isomer, binds only to peripheral cholinergic receptors (12). IDEX readily crosses the blood-brain barrier, has a high mAChR affinity (B max 1.2 pmole/mg), a slow dissociation rate (Kd 5.8 nM) and low nonspecific binding (10). IDEX binds to M1, M2 and M3 receptor subtypes (13). Iodine-123-levetimide uptake, however, reflects nonspecific binding and blood flow effects (14). IDEX has no pharmacological anticholinergic effect in the picomolar doses administered as a radioligand (10).

IDEX can be produced regularly in high yield (50%–70%) and high specific activity (2000 mCi/ $\mu\text{mole}$ ) and is therefore well suited to clinical SPECT study of human

---

Received Sept. 2, 1994; revision accepted Mar. 6, 1995.

For correspondence contact: Karyn L. Boundy, MD, Dept. of Nuclear Medicine, The Queen Elizabeth Hospital, Woodville Rd., Woodville, SA 5011, Australia.

For reprints contact: Leighton R. Barnden, PhD, Dept. of Nuclear Medicine, The Queen Elizabeth Hospital, Woodville Rd., Woodville, SA 5011, Australia.

mAChR. We have assessed the human radiation dosimetry and confirmed the previous report of cerebral uptake and regional cerebral distribution (14) of  $^{123}\text{I}$ -IDEX SPECT in normal elderly subjects.

## METHODS

### Subjects

Ten normal volunteers, age 60–70 yr, (7 men, 3 women) with no significant medical history were recruited by a local advertisement. Neurological examination, neuropsychological evaluation and  $^{99\text{m}}\text{Tc}$ -HMPAO SPECT showed no abnormalities. No subjects were on any medication with anticholinergic properties. After written informed consent was obtained, each subject was given 1.5 g of oral SSKI 30 min prior to injection of 110–150 MBq (3–4 mCi) of IDEX. Four subjects were used for dosimetry calculation and to measure regional cerebral activity over 24 hr. All ten subjects were used to calculate regional cerebral IDEX distribution 6 hr postinjection.

### Radionuclide Production

Iodine-123 was produced with ultrahigh purity using the reaction:



by the National Medical Cyclotron, Sydney, Australia. The radionuclidic purity of each dose exceeded 99.8%.

### Radlolligand Production

Iodine-123-4-iododexetimide was prepared by the Australian Nuclear Science and Technology Organization, Sydney, Australia and (S)-(+)-3-phenyl-3-(4-piperidinyl)-2,6-piperidinedione ((S)-nordexetimide) was prepared by modification of the previously published protocol of Wilson et al. (10). Aqueous sodium [ $^{123}\text{I}$ ]iodide in (0.1 M NaOH) was obtained from the National Medical Cyclotron. All purifications were carried out on a HPLC system composed of a Rheodyne 7125 injector (Alltecht, Australia), a 510 Waters pump (Waters, Australia), a Waters 440 UV detector and a modified Berthold LB 506 radioactivity detector (Berthold, Australia) with a sodium iodide crystal on a Waters u-Bondapak C-18 10- $\mu$  7.8  $\times$  300 mm column. The analytical system composed of a Rheodyne 7125 injector, a Waters pump 486 UV detector and a Berthold L8 506 radioactivity detector with a sodium iodide crystal and a Goldpak 4.6  $\times$  250 mm C18 10- $\mu$  column.

Aqueous sodium iodide was dispensed by an automatic dispenser through a cation exchange cartridge until the required activity was collected (0.5 ml, 100–150 mCi). The pH of the solution was approximately 8–10. The solution was evaporated to dryness under reduced pressure at 40° C and the residue treated with a solution of trimethylsilyldexetimide (1 mg) and chloromine T (1.5 mg) in 100  $\mu$ l of trifluoroacetic acid. After 15 min of stirring, the solution was quenched with concentrated aqueous ammonia (120  $\mu$ l, in HPLC buffer (0.5 ml)). The clear reaction mixture was injected onto a preparative HPLC system and eluted with 45:55 acetonitrile/0.1 M ammonium acetate at 2.5 ml/min. The required peak was eluted at 37 min which, upon evaporation of the buffer under reduced pressure and reconstitution with sterile 0.9% sodium chloride, gave the 4- $^{123}\text{I}$ -IDEX in a 50%–70% yield. Sterile filtration through a 0.2- $\mu$  Millipore filter gave the required product greater than 97% radiochemical purity with specific activities greater than 2000 mCi/ $\mu$ mole.

### Instrumentation

All whole-body planar and SPECT scans were acquired on a triple-headed gamma camera system (TRIAD 88, Trionix, Twinsburg, OH) using a 20% centered photopeak window and fitted with a low-attenuation head rest (Tru-Scan Imaging, Annapolis, MD). Gamma camera sensitivities for conversion of counts to activity were measured using activity in a 10-cm diameter petri dish according to the NEMA protocol (15).

### Attenuation Measurement

A whole-body transmission scan was performed immediately pre-injection. An  $^{123}\text{I}$  flood source was positioned below the patient for the 15 min of the acquisition with medium-energy collimators. The attenuation for each organ of interest was obtained from the transmission counts per pixel in the organ as a fraction of the unattenuated counts per pixel outside the body above the shoulder.

### Emission Images

Anterior and posterior planar whole-body scans, each in 15 min duration, were acquired at 0.5, 3, 6 and 24 hr postinjection using medium-energy collimators. The subject was not moved during each pair of anterior and posterior acquisitions.

### Measurement of Organ Activity

Organ activity was calculated from counts in regions of interest (ROIs) in the pair of whole-body scans acquired at each time point. For each subject, an ROI set was created to delineate the organs of interest. After mirroring the posterior views about their long axis, the ROI set was applied to all whole-body images after translation to correct for any difference in subject position at the different acquisition times. The source organs included were brain, heart, spleen, testes, lower large intestine, upper large intestine, small intestine, salivary glands (parotid), liver, thyroid, lungs and urinary bladder. The attenuation-corrected activity  $A(t)$  for each source organ before background subtraction was computed using:

$$A(t) = \frac{1}{S} \times \sqrt{C_A(t) \times C_P(t) \times N_O(t)/N_T(t)}, \quad \text{Eq. 1}$$

where  $S$  is camera sensitivity in counts per megabecquerel;  $C_A(t)$  and  $C_P(t)$  are anterior and posterior emission counts; and  $N_T(t)$  and  $N_O(t)$  are attenuated and unattenuated transmission counts per pixel at time  $t$  postinjection. The organ geometry factor which is usually included in Equation 1 (16) was assumed to be unity.

### Background Subtraction

The rest-of-body activity exceeded 50% of total activity on average so that appropriate organ background subtraction was necessary. This was most important for small organs such as the thyroid and testes, which were observed against a background count level exceeding their own. Three different background subtraction methods were used.

First, for the organs of the trunk, background from underlying and overlying tissue was characterized by the attenuation-corrected geometric mean counts in a ROI positioned over one thigh. This was subtracted, after area normalization, from the organ activity from Equation 1. Second, the same method was used for thyroid background subtraction, but with a background region immediately superior to the thyroid. Third, for the testes and salivary glands which overlap muscular tissue in part only, a fraction of the normalized thigh background derived in the first

method was subtracted. The fraction used was the organ-to-thigh ratio of a tissue thickness measure given by  $\ln(N_O/N_T)$ .

Background was not subtracted for the brain. Organ activities, residence times, organ absorbed doses and effective doses were computed with and without background subtraction.

### Rest-of-Body (Muscle) Activity

Rest-of-body activity  $A_M(t)$  was calculated by subtraction of the organ activity sum at time  $t$  from the whole-body activity at time  $t$  given by the ratio of the geometric mean whole-body counts at time  $t$  relative to  $t_1$  (before any excretion) multiplied by the decay-corrected injection activity at  $t_1$ , i.e.:

$$A_M(t) = \frac{G_T(t)}{G_T(t_1)} \times A_j e^{-\lambda_p t} - \sum_i A_i(t), \quad \text{Eq. 2}$$

where  $G_T(t)$  and  $G_T(t_1)$  are geometric mean total body counts from the whole-body scans at times  $t$  and  $t_1$ ,  $A_j$  is injected activity,  $\lambda_p$  is the physical decay constant, and  $A_i(t)$  is activity in organ  $i$  at time  $t$ . This is valid if the radionuclide depth distribution does not alter appreciably from  $t_1$  to  $t$ . For organ absorbed dose estimations, the rest-of-body activity was considered as muscle activity.

### Residence Time

For each organ in which activity was observed, the activities measured at the four acquisition times were used to calculate cumulative activity. The time-activity curve for each organ was assumed flat from injection to the first time point, linear between the four times sampled, and falling according to physical decay after the last time point. The cumulative activity is therefore given by:

$$A_i = A_{i1}t_1 + \sum_{j=1}^{n-1} 0.5[A_i(t_j) + A_i(t_{j+1})] \cdot [t_{j+1} - t_j] + A_n(t_n)/\lambda_p \quad \text{Eq. 3}$$

where  $A_i$  is the cumulative activity in the  $i^{\text{th}}$  organ,  $A_{i1}$  is activity in organ  $i$  at the first time point,  $t_1$  is the time interval between injection and the first pair of emission images,  $t_j$  is the time interval between injection and the  $j^{\text{th}}$  pair of emission images, and  $n$  is the number of pairs of emission images acquired. Residence times (hr) were derived by dividing the cumulative dose (MBq·hr) by activity injected (MBq).

### Bladder Dose

The bladder wall absorbed dose was calculated using the method described in *ICRP 53 (17)*. This requires  $f$ , the fraction of activity eliminated by the renal system, and  $\lambda_p$  and  $\lambda_b$ , the physical and biological decay constants, which for a single-compartment model for urine excretion are related by:

$$A_B(t) = fA_j e^{-\lambda_p t} [1 - e^{-\lambda_b t}], \quad \text{Eq. 4}$$

where  $A_B(t)$  is the cumulative bladder activity at time  $t$  and  $A_j$  is the injected activity.

These urine excretion parameters were obtained by collecting urine four to six times over 24 hr and fitting the accumulated activity to Equation 4.

### Organ Absorbed Doses

The MIRD schema (18) together with  $S$  factors for  $^{123}\text{I}$  (19) were used to estimate organ absorbed doses for reference man. The absorbed dose for the testes, a source organ, were derived

using data from the male subjects only. Absorbed doses for ovaries, uterus and breast, none of which were source organs, were derived using data from all subjects.

Effective dose and effective dose equivalent were calculated using weighting factors from *ICRP 60 (20)* and *ICRP 53 (17)*, respectively. The five remaining organs with the highest absorbed doses were given weights of 0.01 for the effective dose and 0.06 for effective dose equivalent. Results for men and women were averaged.

### Brain SPECT

Brain SPECT images were acquired with low-energy ultrahigh resolution fanbeam collimators at 1, 3, 6 and 24 hr in four subjects and at 6 hr in all ten subjects. SPECT data were acquired at 72 angles, into a  $128 \times 64$  matrix (3.56 mm pixel size), for 30 sec per view. The fanbeam projection set was rebinned to simulate images acquired with a parallel-hole collimator. The rebinned projection set was then prefiltered in two dimensions with a Metz filter with the one-dimensional form:

$$M(f) = \text{MTF}^{-1}(f) \{1 - [1 - H^2(f)]^X\},$$

in which MTF is the modulation transfer function derived from the rebinned point spread function of an  $^{123}\text{I}$  point source 90 mm from the camera face and 35 mm deep in a 150-mm diameter lucite phantom.  $H(f)$  is the generalized exponential MTF (21) optimized for  $^{99\text{m}}\text{Tc}$  15 cm from the camera and 7.5 deep in a phantom.  $X$  is the factor which controls the extent to which the inverse filter is followed before the Metz filter switches to noise suppression (in this instance  $X = 200$ ). These prefiltered projections were then reconstructed using filtered backprojection (ramp filter only) incorporating slice-specific elliptical contour Chang attenuation correction with attenuation coefficient 0.14/cm.

### Quantification of SPECT Data

Sections parallel to the plane of the inferior surface of the frontal and occipital lobes were generated from the raw transaxial sections. For quantification purposes, two adjacent transverse slices at the level of maximal basal ganglia activity were added to yield a 7.12-mm thick slice. An ROI template was generated for the striatum, thalamus, and the frontal, parieto-temporal and occipital cortex. Each ROI in the template could be moved independently if adjustments were necessary for individual patients. Each ROI was contracted in to the level of 30% of the maximum count in that region. Mean counts per pixel for each ROI were used to calculate ratios between selected ROI pairs. Count levels for the cerebellum were obtained from a midline sagittal image by the same method.

## RESULTS

### Dosimetry

Whole-body images (Fig. 1) revealed persistent high brain and liver uptake with lower uptake in the lungs, heart and gut. A moderate level of background activity remained visible for the 24 hr of observation. Renal clearance yielded activity in the bladder. Low levels of activity were noted in the testes, thyroid and salivary glands. Figure 2 shows time-activity curves for rest-of-body, liver, brain, upper large intestine, lungs and heart and demonstrates the slow washout rate of brain activity.

Table 1 lists residence times for the source organs iden-

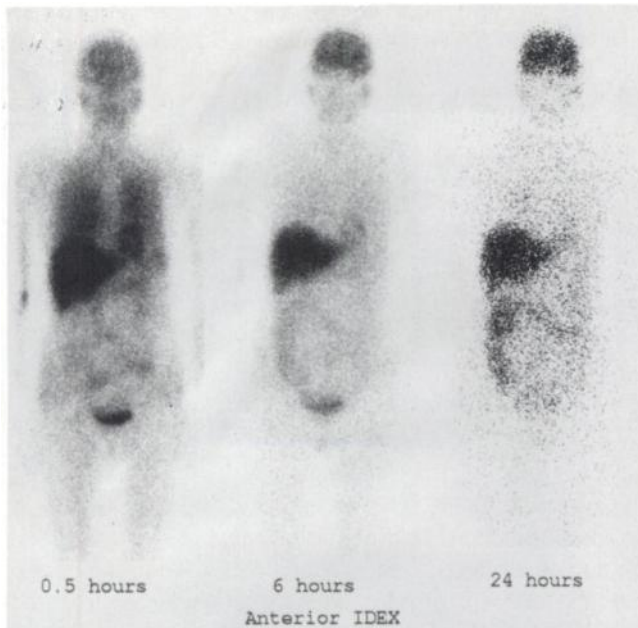


**FIGURE 1.** Anterior whole-body IDEX scans at 0.5, 6 and 24 hr in a normal woman. Counts are displayed in the 0.5- and 6-hr scans scaled to a common maximum. Counts displayed in the 24-hr scan are enhanced relative to the other two. There is persistent activity in the liver, brain, colon and body background.

tified. This parameter multiplied by activity injected (MBq) yields cumulative dose. Rest-of-body, liver, brain, upper and lower large intestine and lung have the highest values. Rest-of-body accounts for 54% of the total.

Without background subtraction, the residence times are greater by 1.2–2.0 for organs in the trunk, 2.0 for the thyroid and 3.5 for the testes.

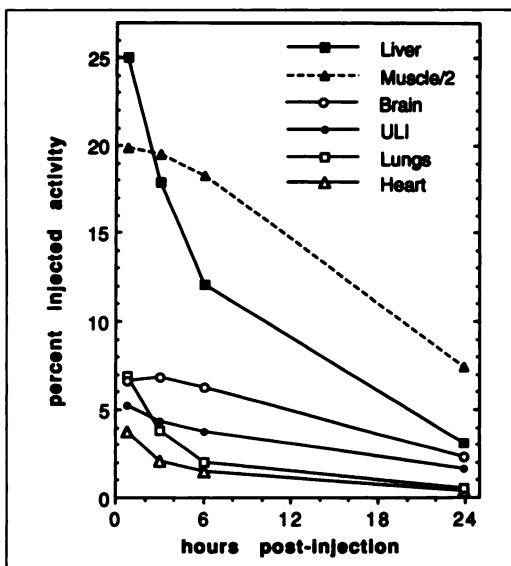


**FIGURE 2.** Time dependence of activity in liver, muscle, brain, upper large intestine, lungs and heart as percentage of injected dose averaged over four subjects. The rest-of-body data, labeled here as muscle, have been divided by two for display in the same range as the other organs.

**TABLE 1**

Mean Iodine-123-IDEX Residence Times (n = 4) in Hours for Source Organs in which Activity Was Observed

Organ	Residence time	s.d.*	Residence time without background subtraction
Rest-of-body†	9.8	1.04	6.8
Liver	3.1	0.42	3.7
Brain	1.61	0.11	1.61
Upper large intestine wall	1.07	0.075	1.63
Lower large intestine wall	0.64	0.096	1.05
Lungs	0.61	0.38	1.27
Small intestine	0.54	0.13	0.83
Heart wall	0.40	0.10	0.53
Urinary bladder wall	0.15	0.018	0.15
Spleen	0.13	0.035	0.21
Salivary glands	0.037	0.015	0.069
Testes	0.028	0.0045	0.090
Thyroid	0.0066	0.0048	0.079

\*Standard deviation of residence time.

†Applied as muscle in dosimetry.

Twenty percent of IDEX was excreted in the urine with an average biological half-time of 11.2 hr (from  $f$  and  $\lambda_b$  in Equation 4).

In Table 2, target organ absorbed doses, the effective dose and effective dose equivalent are tabulated with and without background subtraction. The highest organ absorbed doses in  $\mu\text{Gy}/\text{MBq}$  were upper large intestine (74), liver (71), lower large intestine (63), and brain (45) and heart wall (41). Effective dose was 24.7  $\mu\text{Sv}/\text{MBq}$  and effective dose equivalent was 28.5  $\mu\text{Sv}/\text{MBq}$ . Without background subtraction, the effective dose was 39.5  $\mu\text{Sv}/\text{MBq}$  and the effective dose equivalent 43.2  $\mu\text{Sv}/\text{MBq}$ .

### Brain Uptake and Distribution

Figure 3 shows brain-activity curves with and without physical decay correction. With decay correction, percent brain uptake was mean 6.9%  $\pm$  0.44% (mean  $\pm$  s.d.) at 1 hr, 8.6% ( $\pm$ 0.45%) at 6 hr and 8.1% ( $\pm$ 0.25%) at 24 hr. Table 3 shows the mean and standard deviation of the decay-corrected normalized regional brain activity over time in four subjects at 1, 3, 6 and 24 hr. The counts in each region were normalized to the sum of counts in all regions at 1 hr.

Regional cerebral IDEX uptake and retention was consistent with the known distribution of mAChR (22), with the highest activity in striatum and cortex, low activity in thalamus and very low activity in the cerebellum at 6 hr. (Table 4). Figure 4 shows decay-corrected counts per pixel for striatum, occipital and frontal cortex, thalamus, and cerebellum from one subject who underwent frequent SPECT studies. All areas except the cerebellum demonstrated a progressive increase in activity peaking after 6 hr. The effect of time on IDEX SPECT images is illustrated by Figure 5.

**TABLE 2**  
Radiation Dose Estimates for Iodine-123-Iododexetimide for Adult Reference Man

Organ	Absorbed dose $\mu\text{Gy}/\text{MBq}$	Absorbed dose
		$\mu\text{Gy}/\text{MBq}$ without background subtraction
Upper large intestine wall*†	73.6	107
Liver*	71.3	84.5
Lower large intestine wall*	63.0	96.7
Brain*†	45.0	44.8
Heart wall*	41.2	52.3
Small intestine†	31.9	44.1
Spleen†	28.5	40.4
Lungs	24.7	40.5
Bladder wall	22.9	22.4
Testes	23.0	60.4
Ovaries	19.9	24.5
Bone surfaces	15.7	14.9
Thyroid	15.3	79.7
Pancreas†	15.2	16.3
Muscle	14.9	12.7
Adrenal	14.8	15.8
Uterus	14.2	15.2
Kidneys	11.9	12.6
Stomach	11.3	12.2
Bone marrow	8.6	9.0
Female breasts	4.4	4.9
EDE ( $\mu\text{Sv}/\text{MBq}$ )	28.5	43.2
Effective dose ( $\mu\text{Sv}/\text{MBq}$ )	24.7	39.5

\*Remainder organs for effective dose equivalent (EDE).

†Remainder organs for effective dose.

## DISCUSSION

Because about half of IDEX activity in humans resides in background tissue, background subtraction has a strong influence on the dosimetry results, particularly for small organs such as thyroid and testes observed against a sig-

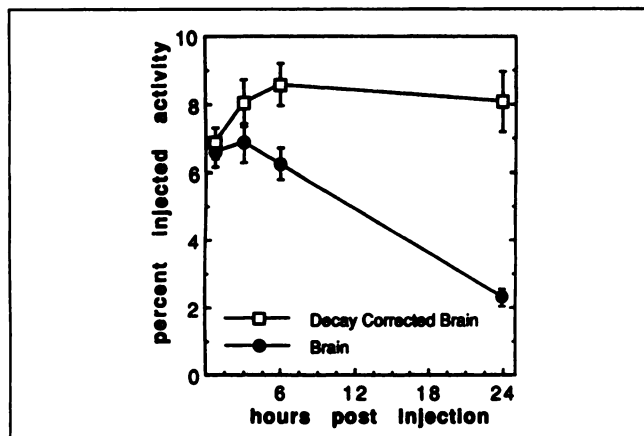


**FIGURE 3.** Time dependence of whole-brain activity averaged over four normal subjects. The lower curve is the measured activity as a percentage of injected activity. The upper curve is the same data corrected for  $^{123}\text{I}$  physical decay.

**TABLE 3**  
Decay-Corrected Normalized Regional Brain Activity\* over Time in Four Subjects

Region	1 Hr		3 Hr		6 Hr		24 Hr	
	Mean	s.d.	Mean	s.d.	Mean	s.d.	Mean	s.d.
Striatum	15.4	0.8	18.3	0.29	18.6	3.0	19.7	†
Frontal	10.5	0.49	11.4	0.92	12.0	1.1	11.6	2.8
Parietal	10.3	0.2	11.2	0.45	12.2	2.2	11.7	2.8
Occipital	15.5	1.4	18.1	2.1	17.6	1.8	15.7	2.8
Thalamus	11.2	1.3	10.5	2.4	8.1	3.7	6.2	1.1
Cerebellum	6.9	1.7	4.5	0.61	4.5	1.7	2.9	2.1

\*Normalized to sum of counts in all regions at one hour.

nificant background. The widespread uptake of IDEX in organs throughout the trunk meant that the conventional method of subtracting background measured in the immediate vicinity of an organ could only be applied here for the thyroid. Normalized thigh activity, adopted here as representative of organ background, assumes that the sum of the background tissue bulk above and below each source organ is the same as in the thigh. In the absence of detailed individual anatomy from CT or MRI, we believe this is the best approach available.

### Background Subtraction

The method described here for background subtraction from organs only partially overlying background tissue (testes and salivary glands), based on the ratio of tissue thickness at the organ-to-tissue thickness at the thigh on the transmission scan, only applies to small organs for which overlying tissue is only background. If background is not subtracted, the organ absorbed dose is increased by more than 5 times for the thyroid, about 3 times for the testes and up to 60% for organs of the trunk.

The reasons for persistent background activity are unclear and may include blood-pool activity, nonspecific binding and binding to the mAChR in the smooth muscle of the endothelial lining of blood vessels. Background activity was assigned to muscle as a "source organ" for organ absorbed dose estimation.

High brain uptake at 6 hr (8.6% of injected dose corrected for decay) permits images of high quality to be

**TABLE 4**  
IDEX Brain Distribution in Ten Normal Subjects at Six Hours\*

	Mean	s.d.
Frontal cortex	0.69	0.05
Parietal cortex	0.70	0.04
Occipital cortex	1.02	0.09
Thalamus	0.54	0.08
Cerebellum	0.11	0.07

\*Ratios relative to striatum derived using mean pixel count in regions with 30% threshold.

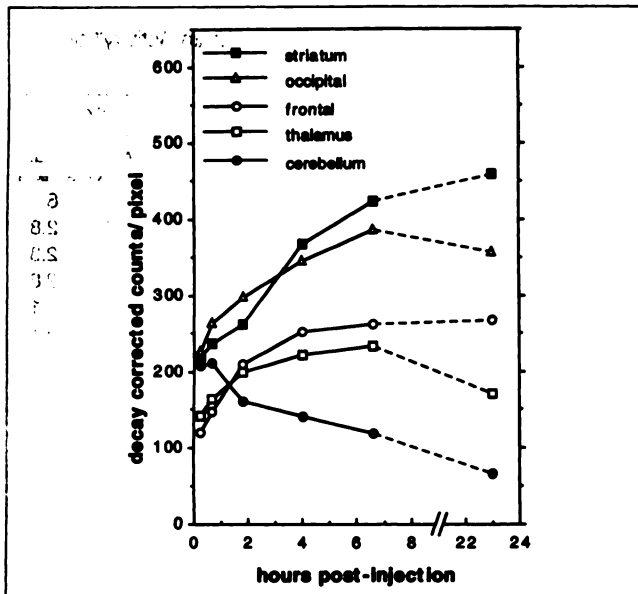


**FIGURE 4.** Time dependence in one normal subject of activity in the striatum, occipital cortex, frontal cortex, thalamus and cerebellum to 24 hr postinjection. The average count per pixel in regions contracted to 30% of the maximum pixel count in each ROI is shown. Between 0.5 and 6 hr the half clearance time for cerebellar activity is 3.6 hr.

obtained with as little as 100 MBq (3 mCi) with a 40-min acquisition on a triple-head camera so that normal subjects can be studied within accepted dose limits.

The effective dose equivalent (EDE) for IDEX is 28.5  $\mu\text{Sv}/\text{MBq}$ . This yields 5.3 mSv from a typical injection of 185 MBq (5 mCi). For comparison, the EDE for  $^{99\text{m}}\text{Tc}$ -HMPAO is 8.3  $\mu\text{Sv}/\text{MBq}$  (23), so that a typical dose of 740 MBq yields an EDE of 6.1 mSv. The EDE of IDEX is higher than that reported for some  $^{123}\text{I}$  agents, for example, the 11.4  $\mu\text{Sv}/\text{MBq}$  of the D2 receptor agent  $^{123}\text{I}$ -iodoben-

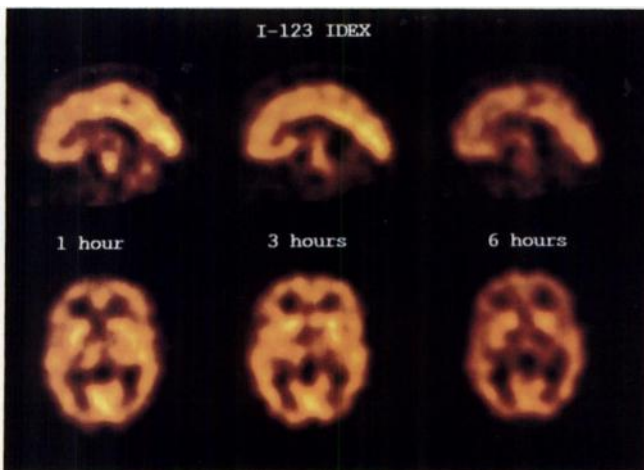


**FIGURE 5.** IDEX-SPECT midline sagittal (top row) and transverse (bottom row) sections at 1, 3 and 6 hr postinjection. The transverse sections pass through the basal ganglia and are parallel to the plane of the inferior surface of the frontal and occipital lobes. All images are scaled to a common maximum pixel count. Slice-specific attenuation correction was applied.

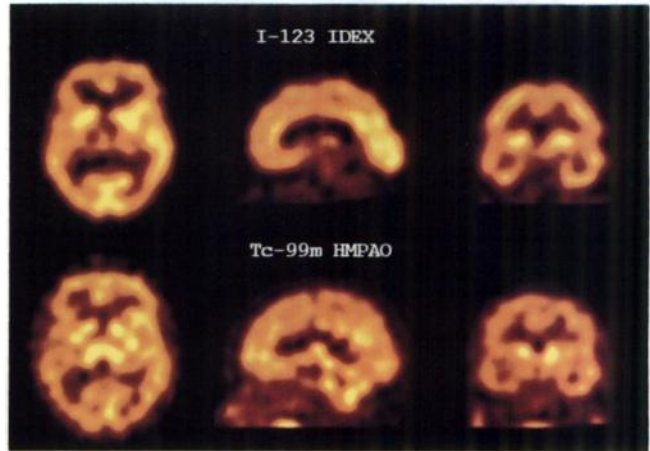


**FIGURE 6.** Comparison of SPECT sections in the same normal subject of an IDEX scan 6 hr postinjection and a HMPAO scan 0.5 hr postinjection. Notice the difference in the relative uptake in the thalamus and cerebellum.

zamide (24), but similar to the EDE of 33  $\mu\text{Sv}/\text{MBq}$  for the benzodiazepine receptor ligand  $^{123}\text{I}$ -iomazenil.

IDEX has several advantages over the other available muscarinic ligand,  $^{123}\text{I}$ -QNB. Radioiodinated 4-IQNB is prepared by the nucleophilic attack of radioiodide on a phenylonium intermediate produced by the acid catalyzed decomposition of a triazene intermediate, which does not produce a high yield (15%–20%). Consequently, radioligands produced by these reactions are very expensive to prepare in quantities sufficient to produce good image quality (22).

We have regularly produced IDEX in high yield (50%–70%) with high specific activity in amounts of 300–550 MBq (8–15 mCi), quantities suitable for clinical studies, and have now performed over 60 human studies in several research protocols. As expected, no adverse pharmacological effects have resulted from the use of IDEX in these 60 subjects.

IDEX is stable for at least 20 hr from the time of production. It was produced in the afternoon prior to use, transported 1200 km from Sydney to Adelaide, injected into two or three subjects at 9 am and SPECT scans were performed 6 hr later. Most scans have been of good quality, but some lower activity studies were count-deficient so an injection activity of 185 MBq is recommended.

#### Regional Concentration of IDEX

Regional brain concentration of IDEX changes markedly over the first 4–6 hr postinjection. Activity in areas known to contain high concentrations of mAChR such as the striatum and cortex demonstrated increasing activity. Total brain uptake rose from 6.8% ( $\pm 0.46\%$ ) at 1 hr to a maximum of 8.6% ( $\pm 0.42\%$ ) at 6 hr and 8.07% ( $\pm 0.88\%$ ) at 24 hr. These results confirm an earlier study that reported peak regional brain activity at 7–12 hr with subsequent plateau of activity. It appears that high initial uptake and subsequent release from organs such as the liver and lungs provides sufficient blood concentration to permit continued

uptake in the brain in the first few hours. The cerebellum, which contains a low concentration of mAChR (14,22) showed moderate IDEX activity at 1 hr. By 6 hr, however, cerebellar activity was minimal, suggesting that initial blood flow distribution effects and nonspecific uptake can be minimized though not eliminated by delayed imaging. For these reasons and because it was clinically convenient, 6 hr postinjection was chosen as the optimal time for SPECT acquisition for subsequent clinical studies.

Figure 6 compares IDEX-SPECT at 6 hr with HMPAO-SPECT in the same subject. Clear differences are seen in the cerebellar and thalamic activity. The 6-hr IDEX-SPECT image with high activity in the striatum and cortex, low activity in thalamus and very low activity in the cerebellum is consistent with the known distribution of mAChR (22) and with the earlier report of Muller-Gartner et al. (14). Although frontal and parietal cortical activity measured less than the striatum or occipital cortex in our study, conclusions about the actual relative concentration of mAChR cannot be drawn without correction for partial volume effects. The thickness of the frontal and parietal cortex in the image used for analysis was less than the resolution of our imaging system, so a significant underestimation of activity in these areas will have occurred. The relative uptake of frontal cortex to striatum was greater in the study of Muller-Gartner et al. (14), where MRI-based partial volume correction was performed.

In comparison to IDEX, the brain uptake of  $^{123}\text{I}$ -QNB is even more prolonged with peak count rates occurring more than 16 hr after injection, and the striatal-to-cerebellar activity ratio rising for up to 48 hr (7). The striatal-to-cerebellar ratio at 6 hr for IDEX was 11%, while for QNB it has been reported as 30% at 2 hr and 7% at 15 hr (7).

Our study has shown the biodistribution of  $^{123}\text{I}$ -IDEX in normal elderly subjects and demonstrated that this compound has acceptable dosimetry for human use. The regional brain distribution of IDEX reflects known mAChR distribution, as described by Muller-Gartner et al. (14).

## CONCLUSION

Iodine-123-IDEX has significant production advantages over  $^{123}\text{I}$ -QNB and is a suitable agent for large clinical studies of pathological conditions that involve the cholinergic system such as Alzheimer's disease, Parkinson's disease, temporal lobe epilepsy, dystonia and Huntington's chorea.

## ACKNOWLEDGMENTS

This work was supported by the Australian Brain Foundation and a University of Adelaide Postgraduate Medical Research Scholarship (KLB).

## REFERENCES

- Bartus RT, Dean RL, Beer B, Lippa AS. The cholinergic hypothesis of geriatric memory dysfunction. *Science* 1982;217:408-427.
- Agid Y, Ruberg M, Dubois B, Pillon B. Anatomoclinical and biochemical concepts of subcortical dementia. In: Stahl SM, Iversen SD, Goodman EC, eds. *Cognitive neurochemistry*. Oxford: Oxford University Press; 1987: 248-271.
- Khalili-Varasteh M, Brouillet E, Chariox C, et al. Caractérisation des récepteurs cholinergiques centraux chez la babouin vivant par tomographie par émission de positrons. *J Med Nucl Biophysique* 1988;12:400-401.
- Dewey SL, Bendriem B, Macgregor B, et al. PET studies using (11-C) cogentin in baboon brain. *J Cereb Blood Flow Metab* 1989;9(suppl 1):S13.
- Frey KA, Koeppe RA, Mulholland GK, et al. Muscarinic receptor imaging in human brain using (C-11)scopolomine and positron emission tomography [Abstract]. *J Nucl Med* 1988;29:808.
- Wilson AA, Scheffel UA, Dannals RF, Sthathis M, Ravert HT, Wagner HN Jr. In vivo biodistribution of two ( $^{18}\text{F}$ )- and 4-( $^{18}\text{F}$ )-fluorodexetimide. *Life Sci* 1991;48:1385-1394.
- Holman BL, Gibson RE, Hill TC, Eckelman WC, Albert M, Reba RC. Muscarinic acetylcholine receptors in Alzheimer's disease. *JAMA* 1985;254: 3063-3066.
- Weinberger DR, Gibson R, Coppola R, et al. The distribution of cerebral muscarinic receptors in-vivo in the patients with dementia. *Arch Neurol* 1991;48:169-176.
- Rzeszotarski WJ, Eckelman WC, Francis BE, et al. Synthesis and evaluation of radioiodinated derivatives of 1-azabicyclo (2,2,2) oct-3-yl alpha-hydroxy-alpha-(3-iodophenyl) phenylacetate as potential radiopharmaceuticals. *J Med Chem* 1984;27:1156-1158.
- Wilson AA, Dannals RF, Ravert HT, Frost JJ, Wagner HN Jr. Synthesis and biological evaluation of  $^{123}\text{I}$  and  $^{124}\text{I}$ -iododexetimide, a potent muscarinic cholinergic receptor antagonist. *J Med Chem* 1989;32:1057-1062.
- Laduron PM, Verwimp M, Leysen JE. Stereospecific in vitro binding of H-3-dexetimide to brain muscarinic receptors. *J Neurochem* 1978;32:421-427.
- Laduron PM, Janssen PFM. Characterisation and subcellular localisation of brain muscarinic receptors labelled in vivo by H-3-dexetimide. *J Neurochem* 1979;33:1223-1231.
- Waelbroeck M, Tastenoy M, Camus J, et al. Stereo selectivity of the interaction of muscarinic antagonists with their receptors. *Trends Pharmacol. Sci. 10 (Suppl. Subtypes Muscarinic Recept. IV)* 1989;10(suppl): 60-64.
- Muller Gartner HW, Wilson AA, Dannals RF, et al. Imaging muscarinic cholinergic receptors in human brain in vivo with SPECT,  $^{123}\text{I}$ -4-iododexetimide. *J Cereb Blood Flow Metab* 1992;12:562-570.
- NEMA. Performance measurements of scintillation cameras. In: *NEMA standards publication NU1-1994*. 1994:20.
- Thomas SR, Maxon HR, Keriakes JG. In vivo quantitation of lesion radioactivity using external counting methods. *Med Phys* 1976;3:253-255.
- International Commission on Radiological Protection. *Radiation dose to patients from radiopharmaceuticals, ICRP publication 53*. Oxford: Pergamon; 1988:18-19.
- Loevinger R, Budinger TF, Watson EE. *MIRD primer for absorbed dose calculations*. New York: Society of Nuclear Medicine; 1991:1-21.
- Stabin MG. *MIRDOSE3*. Radiation Internal Dose Information Center, Oak Ridge Institute for Science and Education, Oak Ridge, TN, 1994.
- International Commission on Radiological Protection. *1990 recommendations of the international commission on radiological protection, ICRP Publication 60*. Oxford: Pergamon Press; 1990:6-8.
- King MA, Schwinger RB, Penney BC. Variation of the count-dependent Metz filter with imaging system modulation transfer function. *Med Phys* 1986;13:139-149.
- Davies P, Verth AH. Regional distribution of muscarinic acetylcholine receptor in normal and Alzheimer's type dementia brains. *Brain Res* 1979; 138:389-392.
- Soundy RG, Tyrell DA, Pickett RD, Stabin M. The radiation dosimetry of technetium-99m-exametazine. *Nucl Med Commun* 1990;11:791-799.
- Kung HF, Alavi A, Chang W. In vivo SPECT imaging of CNS D-2 dopamine receptors: initial studies with iodine-123-IBZM in humans. *J Nucl Med* 1990;31:573-579.